

# Fluctuation-dissipation relations in plaquette spin systems with multi-stage relaxation

Robert L Jack<sup>1,2</sup>, Ludovic Berthier<sup>3</sup> and Juan P Garrahan<sup>4</sup>

<sup>1</sup> Rudolf Peierls Centre for Theoretical Physics, University of Oxford, 1 Keble Road, Oxford, OX1 3NP, UK

<sup>2</sup> Department of Chemistry, University of California, Berkeley, California 94720-1460, USA

<sup>3</sup> Laboratoire des Colloïdes, Verres et Nanomatériaux, UMR 5587 Université Montpellier II & CNRS, 34095 Montpellier Cedex 5, France

<sup>4</sup> School of Physics and Astronomy, University of Nottingham, Nottingham, NG7 2RD, UK

E-mail: rljack@berkeley.edu, berthier@lcvn.univ-montp2.fr,  
juan.garrahan@nottingham.ac.uk

**Abstract.** We study aging dynamics in two non-disordered spin models with multi-spin interactions, following a sudden quench to low temperature. The models are relevant to the physics of supercooled liquids. Their low temperature dynamics resemble those of kinetically constrained models, and obey dynamical scaling, controlled by zero-temperature critical points. Dynamics in both models are thermally activated, resulting in multi-stage relaxation towards equilibrium. We study several two-time correlation and response functions. We find that equilibrium fluctuation-dissipation relations are generically not satisfied during the aging regime, but deviations from them are well described by fluctuation-dissipation ratios, as found numerically in supercooled liquids. These ratios are purely dynamic objects, containing information about the nature of relaxation in the models. They are non-universal, and can even be negative as a result of activated dynamics. Thus, effective temperatures are not well-defined in these models.

## 1. Aging dynamics and plaquette models

When a liquid is cooled through its glass transition, its state changes: it becomes an amorphous solid [1]. In this non-equilibrium state, physical properties are not stationary, and the system displays aging behaviour [2, 3]. A similar situation is encountered in many different materials, ranging from disordered magnets to dense granular media. A full understanding of the non-equilibrium glassy state remains a central theoretical challenge. In this work, we study the aging dynamics of two spin models with multi-spin interactions [4]. These finite-dimensional, non-disordered, dynamically heterogeneous systems have been of recent interest as models for the glass transition in supercooled liquids [5, 6, 7].

Theoretical studies of mean-field models have given important insights into the aging dynamics of both structural and spin glasses [8]. In these models, thermal equilibrium is never reached, and aging proceeds by downhill motion in an increasingly flat free energy landscape [9]. Time translational invariance is broken, and two-time correlation and response functions depend on both their arguments. The fluctuation-dissipation theorem (FDT), which relates equilibrium correlation and response functions, does not apply in the aging regime. Instead, correlation and response are related by a non-trivial fluctuation-dissipation ratio (FDR). This led to the idea that aging systems might be characterised by an effective temperature [10], defined in terms of the FDR. Physically, relaxation in glassy systems occurs in well-separated time sectors; it is easy to imagine associating each sector with an effective temperature [11]. A thermodynamic interpretation of effective temperatures has also been suggested [8, 12], related to the concept of replica symmetry breaking. Taken together, these results lend considerable appeal to the the mean-field description of aging (see [13] for a review).

However, there are many systems of physical interest in which the dynamics are not of mean-field type, displaying both activated processes and spatial heterogeneity. Two examples are domain growth in disordered magnets [14], and liquids quenched to below the glass transition [15, 16]. While some experiments and simulations [13] seem to detect a mean-field aging regime, theoretical studies have found ill-defined FDRs [17], non-monotonic response functions [5, 18, 19, 20, 21], observable dependence [22, 23], non-trivial FDRs without thermodynamic transitions [5], and a subtle interplay between growing dynamical correlation length scales and FDT violations [24, 25]; experiments have also detected anomalously large FDT violations associated with intermittent dynamics [26]. Moreover, at large times, aging often proceeds via thermal activation, and it was recently shown [27] that this can lead to negative response and well-defined, but negative, FDRs.

In this work, our aim is to investigate further the effects of thermal activation and dynamic heterogeneity on aging dynamics. To this end, we study two different two-dimensional plaquette models with multi-spin interactions [4, 5, 6, 7, 21, 28, 29]. On one hand, they can be viewed as finite dimensional, non-disordered versions of  $p$ -spin models, and can be viewed as an attempt to transfer mean-field concepts to the finite

dimensional world. On the other hand, they possess dual representations in terms of independent plaquette excitations with constrained dynamics, and are therefore directly related to the physics of kinetically constrained models (KCMs) [30], with the advantage that both spin and excitation degrees of freedom can be studied separately [31].

In these models, low temperature relaxation towards equilibrium proceeds via several distinct stages, each stage being associated with a particular energy barrier. While these separate time scales are superficially reminiscent of the time sectors found in mean-field spin glasses, their physical origin is quite different. We will show that the dynamics of plaquette models share some strong similarities with mean-field aging dynamics, but also important differences. In addition, the dynamics of these models becomes critical at low temperatures, where dynamical length scales diverge. Our work therefore also pertains to the study of FDRs in non-equilibrium critical dynamics [13, 32].

The first model that we study is the triangular plaquette model (TPM) [4, 21, 29], defined for Ising spins,  $s_i = \pm 1$ , on the vertices of a triangular lattice. The Hamiltonian is

$$H_{\text{TPM}} = -\frac{1}{2} \sum_{1,2,3 \in \nabla} s_1 s_2 s_3, \quad (1)$$

where the sum is over the downward pointing triangular plaquettes of the lattice. We work with periodic boundary conditions in a system of linear size  $L$  of the form  $L = 2^k$ . The dynamics involve single spin flips, with Glauber rates.

It is useful to define the binary dual plaquette variables by

$$n_i \equiv \frac{1}{2}(1 - s_1 s_2 s_3), \quad (2)$$

where the three spins lie on the vertices of the  $i$ th downward-pointing triangular plaquette. The thermodynamics of the system are those of the  $L^2$  non-interacting dual spins  $n_i$ . Combining (1) and (2) we have, at temperature  $T = \beta^{-1}$ , the equilibrium defect density,  $\langle n_i \rangle_{\text{eq}} = (1 + e^\beta)^{-1}$ , and an obvious connection to kinetically constrained models [4, 21].

The TPM has a hierarchical free energy landscape: as the temperature is lowered, the system falls into ever deeper potential wells, and the equilibrium relaxation time diverges as  $\tau \sim e^{\beta^2/\ln 3}$  [7]. This behaviour resembles that of the one-dimensional East model [33], or its generalization in higher dimensions [34, 35]. The hierarchy of energy barriers in the TPM is clear from the behaviour on a quench: in Fig. 1, we plot the defect (or energy) density

$$c(t) \equiv \langle n_i(t) \rangle, \quad (3)$$

as a function of time, after a quench from infinite temperature (the average is over initial conditions and over thermal histories). The energy barriers relevant for the quench take integer values, so the decay of the energy becomes a function of the scaling variable  $T \log t$ , as long as  $t$  remains smaller than the equilibration time [36].

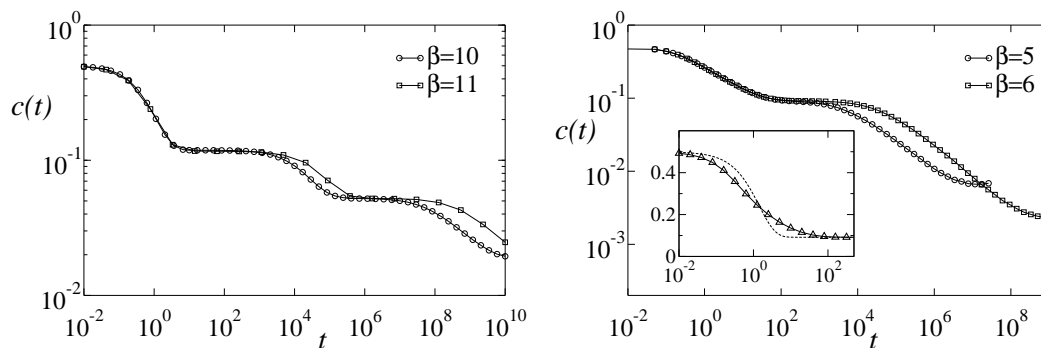


**Figure 1.** Relaxation of the energy density in the TPM (left) and SPM (right), after a quench from infinite temperature to  $T = \beta^{-1}$ . In the TPM, the relaxation proceeds in a hierarchical way, with stages corresponding to integer energy barriers [6, 21]. The system has not yet equilibrated: this will occur when  $c(t) = (1 + e^\beta)^{-1}$ . In the SPM, the decay has just two stages; the second plateau in the decay of  $c(t)$  represents equilibration of the system. The first stage of relaxation has no energy barriers, and corresponds to zero temperature dynamics (a quench to  $T = 0$  is shown in the inset, and compared with a simple exponential as a dashed line); the second step is characterised by activated reaction-diffusion behaviour [6].

Our second system is the square plaquette model (SPM) [28, 4], in which we define Ising spins  $s_i = \pm 1$  on a square lattice, with

$$H = -\frac{1}{2} \sum_{1,2,3,4 \in \square} s_1 s_2 s_3 s_4, \quad (4)$$

where the sum is over the elementary plaquettes of the square lattice. For the SPM, we define the binary dual variables by

$$n_i \equiv \frac{1}{2}(1 - s_1 s_2 s_3 s_4), \quad (5)$$

where the four spins lie on the vertices of the  $i$ th square plaquette. We use the same symbol,  $n_i$ , for the dual spins in both plaquette models. The thermodynamics are again those of non-interacting dual spins, but constraints from the boundary conditions cannot be avoided in this model [7]. These are minimised by our use of periodic boundary conditions, but it is necessary to use linear system sizes  $L$  significantly greater than the inverse density of defects,  $L\langle n_i \rangle \gg 1$ . This is a rather strong constraint at low temperature. In the thermodynamic limit, the equilibrium defect density is the same as that of the TPM,  $\langle n_i \rangle_{\text{eq}} = (1 + e^\beta)^{-1}$ .

The low temperature behaviour in the SPM is that of dilute point defects. In equilibrium, they diffuse at a rate that is proportional to  $e^{-3\beta}$ ; similar activated diffusion occurs in the Fredrickson-Andersen (FA) model [37]. This process is mediated by pairs of defects that diffuse rapidly along one-dimensional paths that are aligned with the lattice axes. Where the TPM has a hierarchical relaxation towards equilibrium, the SPM has just two stages. The behaviour on a quench is shown in Fig. 1. The second stage is a reaction-diffusion process with activated diffusion, and the decay is a function of the rescaled time  $te^{-2\beta}$  [5, 6]. The early time regime of the SPM has no energy

barriers. It corresponds to relaxation into a jammed state at zero temperature. This relaxation is frustrated by entropic effects leading to a non-exponential relaxation of the energy density, as shown in the inset of Fig. 1.

Earlier work on aging dynamics in the TPM and SPM [5, 21] suggested that the combination of activated dynamics and hierarchical relaxation leads to novel and intriguing behaviour for response functions and FDRs. Here, we study these FDRs by computer simulations. We investigate spin and defect observables, including both local and spatially dependent correlations; we make use of a recently developed method for direct measurement of response functions in Monte Carlo simulations [38, 39].

We find a rich structure in the FDRs, with qualitatively different behaviour in different stages of the relaxation. We observe FDRs close to unity for regimes in which energy conserving processes allow the system to explore configuration space efficiently; correlations may also relax by irreversible processes, whose rates are independent of the perturbing field; in this case the FDR is close to zero. The relative rates for these processes reflect local properties of the free energy landscapes in these systems [9]. We also observe negative FDRs, coming from activated aging behaviour, as in [27].

The rest of the paper is organized as follows: in Section II we study FDRs in the triangular plaquette model; in Section III we do the same for the square plaquette model; Section IV gives a brief summary of our results and their implications. Details of the no-field method for measuring response functions are provided in Appendix A.

## 2. Fluctuation-dissipation relations in the triangular plaquette model

### 2.1. Spin observables

We begin by considering correlation and response functions for spins in the TPM. The two-time spin autocorrelation function is

$$C_s(t, t_w) = \langle s_i(t) s_i(t_w) \rangle, \quad (6)$$

and its conjugate response is

$$\chi_s(t, t_w) = \frac{d}{d(\beta h_i)} \langle s_i(t) \rangle, \quad (7)$$

where  $h_i$  is the strength of a magnetic field that acts on site  $i$  between times  $t_w$  and  $t$ . Averages are performed over realisations of the initial condition and the thermal history, as above. For these observables, the FDR,  $X_s(t, t_w)$ , is defined by

$$\left. \frac{\partial \chi_s(t, t_w)}{\partial t_w} \right|_t = -X_s(t, t_w) \left. \frac{\partial C_s(t, t_w)}{\partial t_w} \right|_t. \quad (8)$$

In equilibrium, the fluctuation-dissipation theorem states that  $X(t, t_w) = 1$  for all  $t$  and  $t_w$ . However, away from equilibrium, there are no such restrictions, as we shall see.

Following Refs. [38, 39], two-time linear response functions can be computed without using a perturbing field (see Appendix A for details). This allows direct access to the FDR. We emphasize that the derivatives in Eq. (8) are with respect to  $t_w$ . For

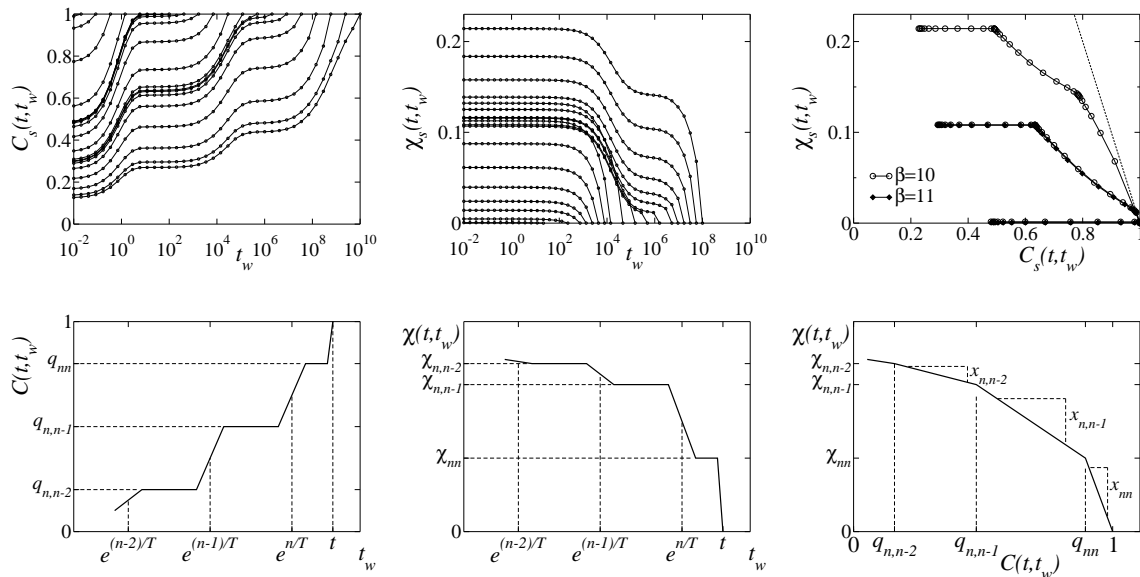


**Figure 2.** (Top) Two-time spin autocorrelations (left), response functions (centre) and parametric FD plots (right) in the TPM at  $\beta = 10$ . The correlation and response are plotted against  $t_w$ , for various  $t$ . The FD plot (top right) uses  $t_w$  as a parametric variable; the three traces at  $\beta = 10$  are  $t = (70, 1.6 \times 10^6, 10^8)$ . The equilibrium FD relation,  $\chi(t, t_w) = 1 - C(t, t_w)$ , is shown as a dashed line. We also show parametric plots for  $\beta = 11$  and  $t = (70, 1.7 \times 10^7)$ . Since these values of  $t$  are within plateaux of  $c(t)$ , the FDR depends very weakly on temperature, although the correlation and response have quite different time dependence (not shown). (Bottom) Sketches of these plots, illustrating the various definitions given in the text. Note that the parameters  $x_{nm}$  label the gradient of the parametric plot.

this reason, we present data for fixed time  $t$ , as a function of  $t_w$ , unlike previous work on the same models where the opposite convention was used [5, 21]. We shall see that this difference qualitatively affects the results and their interpretation.

The dependence of the FDR on  $t_w$  can be replaced by a parametric dependence on the value of the correlation:

$$X(q, t) \equiv X(t, t_w)|_{C(t, t_w)=q}. \quad (9)$$

That is, working at fixed time  $t$ , the waiting time  $t_w$  is parametrised by the value of  $C(t, t_w)$ . A parametric plot of  $\chi(q, t)$  versus  $q$  (an ‘‘FD plot’’) has local gradient  $-X(q, t)$ , corresponding to the FDR defined in Eq. (8). FD plots were suggested by the study of mean-field models where Eq. (9) simplifies to a single argument function  $X(q, t) = \mathcal{X}(q)$ . This asymptotic property has not been confirmed beyond mean-field [13].

The behaviour of the two-time spin autocorrelation function of Eq. (6) is shown in Fig. 2. If  $t$  is held constant, and  $t_w$  decreased, the correlation decreases, in stages that mirror the decay of the energy after the quench (recall Fig. 1). The generic structure of the correlation is sketched in Fig. 2.

The plateaux in the energy,  $c(t)$ , come from the system being trapped in metastable states. The dynamics are effective in exploring the metastable state: in the  $n$ th such

state, events corresponding to energy barriers smaller than  $n$  are very fast, while those corresponding to energy barriers greater than or equal to  $n$  are frozen, until such times that the system escapes from the metastable state. Thus, the autocorrelation function quickly relaxes to a value  $q_{nn}$ , which measures the self-overlap of this metastable state. As  $t_w$  is decreased further, we arrive at a new plateau in the two-time function. This measures the mutual overlap between the plateau state  $n$  and the previous plateau state  $n - 1$ . We denote this quantity by  $q_{n,n-1}$ ; earlier plateaux in the two-time function give the mutual overlaps  $q_{nm}$  with  $m < n$ , see Fig. 2.

The two-time local integrated response,  $\chi_s(t, t_w)$ , is also plotted in Fig. 2. The stages of the dynamics are still visible, although the response decreases with increasing  $t_w$ , unlike the autocorrelation function. Note also that curves for different  $t$  cross one another at short  $t_w$ . This means that response functions plotted at fixed  $t_w$  for increasing  $t$  are non-monotonic, which illustrates why the use of  $t$  as a parametric variable in FD plots produces quite unusual results [17, 21]. We sketch the behaviour of the response function in Fig. 2, and define the plateau values of the response function by  $\chi_{nm}$ . By analogy with the mutual overlap, the mutual response  $\chi_{nm}$  is the value of the response function measured in the stage  $n$ , given that the field was continuously applied from stage  $m$  to stage  $n$ .

If the response is now plotted parametrically against the correlation, then each stage of the dynamics appears as a separate segment on the FD plot. It is clear from Fig. 2 that  $X(q, t) \neq 1$  in the TPM, reflecting the fact that the system is well out of equilibrium. More importantly, it is apparent that the segments of the parametric plot in that figure are close to straight lines, so that FD plots are reducible to a discrete set of numbers. We denote the slopes observed in the FD plots by  $x_{nm}$ , as sketched in Fig. 2. We define

$$x_{nn} = \frac{\chi_{nn}}{1 - q_{nn}}, \quad (10)$$

and

$$x_{nm} = \frac{\chi_{nm} - \chi_{n,m+1}}{q_{n,m+1} - q_{nm}}, \quad (11)$$

for  $n > m$ . These equations are a discretized version of Eq. (8). Physically, each stage  $n$  of the hierarchy corresponds to a given timescale,  $t_n \sim e^{n/T}$ , and a well-defined length scale,  $\ell_n$ , giving rise to well-defined two-time (or rather ‘two-stage’) correlation and response functions and FDRs. The whole dynamical behaviour is therefore encoded in a discrete set of real numbers,  $\{q_{nm}, \chi_{nm}, x_{nm}\}$ , which obey certain relations, as we shall see in section 2.3. The FD plots found for spin observables have similar shapes to the ones reported in Ref. [27] for the East model, but differ significantly from earlier work [21].

The first segment of the response always has a gradient very close to unity,  $x_{nn} \simeq 1$ , consistent with quasi-ergodic (or quasi-equilibrium) dynamics within the metastable plateau state. We also note that the last plateau, which corresponds to correlation and response between stages  $n$  and 0, has  $x_{n0} \simeq 0$ . This is to be expected, since the first stage

of the quench only involves unactivated relaxation events, and these are accepted with a probability close to unity. Thus, their rate depends very weakly on any perturbing field, and the response associated with this completely irreversible dynamics is very weak (more precisely, it is  $\mathcal{O}(e^{-\beta})$ , which does indeed vanish at small temperature). This is very similar to the zero-FDR found in coarsening ferromagnets [40, 41].

We have discussed the data in Fig. 2 at a single temperature. However, the scaling behaviour of the TPM with temperature is well-understood [7, 21]. We find that the plateau values of the energy, the self-overlaps  $q_{nm}$  and the ratios  $x_{nm}$  depend only very weakly on temperature. As the temperature is reduced towards zero, the stages of the dynamics become more clearly defined and timescales more separated. If we plot data as a function of the rescaled times,  $(\nu, \nu_w) = (T \log t, T \log t_w)$ , then the plateaux fall on top of one another, and the parametric plots quickly become independent of temperature (for a given value of  $\nu$ ). This assertion is confirmed numerically in Fig. 2, where we show that parametric plots for different temperatures,  $\beta = 10$  and  $\beta = 11$ , but similar  $\nu$ , perfectly superimpose.

Mean-field studies have suggested the possibility to define effective temperatures from FDRs through [10]

$$T_{\text{eff}}(q) = \frac{T}{\mathcal{X}(q)}. \quad (12)$$

Our finding of piecewise linear FD plots in Fig. 2 apparently offers a nice illustration of the intuitive idea that well-separated relaxation timescales could lead to quasi-thermalization at a given effective temperature within each time sector, as is the case in mean-field spin glasses [8]. A further property derived from mean-field models is that the value of  $T_{\text{eff}}$  is shared by all physical observables, physically implying that different degrees of freedom have also thermalized between themselves. We now investigate this issue.

In the TPM, the spatial dependence of two-spin correlation functions is trivial, since both two-spin correlations and responses are purely local. The symmetries of the model imply [4]

$$\langle s_i(t) s_j(t_w) \rangle = \delta_{ij} C_s(t, t_w), \quad (13)$$

and

$$\frac{d}{dh_i} \langle s_j \rangle = \delta_{ij} \chi_s(t, t_w), \quad (14)$$

which trivially implies that all two-spin correlation functions are equivalent.

In order to study spatial correlations, it would in fact be necessary to consider four-point functions [42]; the relevant correlations were discussed in [7], but we restrict ourselves to two-point functions in this paper. Interestingly, (14) also implies that the dynamics of the total magnetization are trivially related to those of local observables. This remark is potentially relevant for supercooled liquids, where static two-point correlations are also believed to be decoupled from the microscopic physics of cooperative motion.



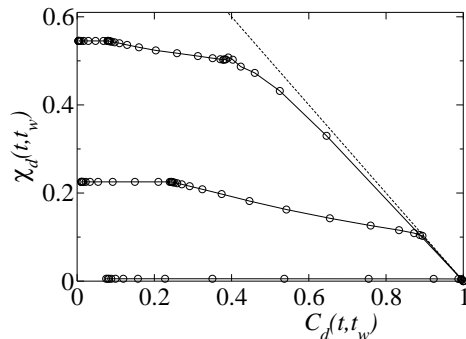


**Figure 3.** Parametric FD plot for defects in the TPM, at  $\beta = 10$  and  $t \in \{70, 1.7 \times 10^6, 10^8\}$ , with  $t$  decreasing from top to bottom. The structure is the same as for the spin observables in Fig. 2, but the FDRs are quantitatively different. The dashed line is the FDT:  $\chi_d(t, t_w) = 1 - C_d(t, t_w)$ .

## 2.2. Defect observables

To understand the significance of the FDRs (and therefore effective temperatures) revealed by spin observables, it is natural to ask whether different physical quantities exhibit a similar behaviour. We therefore consider the dynamics of the dual plaquette variables defined in Eq. (2). An excited plaquette, or “defect”, is a triangular plaquette for which  $n_i = 1$ . Those defects become increasingly dilute at low temperatures. We consider the defect autocorrelation function,

$$C_d(t, t_w) = \frac{\langle n_i(t)n_i(t_w) \rangle - \langle n_i(t) \rangle \langle n_i(t_w) \rangle}{\langle n_i(t) \rangle [1 - \langle n_i(t) \rangle]}, \quad (15)$$

and its conjugate response,

$$\chi_d(t, t_w) = \left[ \frac{d}{d(\beta g_i)} \langle n_i(t) \rangle \right] \frac{1}{\langle n_i(t) \rangle [1 - \langle n_i(t) \rangle]}, \quad (16)$$

where the perturbation  $\delta H = -g_i n_i$  acts between  $t_w$  and  $t$ , and we evaluate the right hand side at  $g_i = 0$ . We use connected correlation functions and we have normalised both correlation and response, so that  $C_d(t, t) = 1$ ,  $C_d(t \rightarrow \infty, t_w) = 0$ , and the fluctuation-dissipation theorem for equilibrated systems reads  $\chi_d(t, t_w) = 1 - C_d(t, t_w)$ .

Overall, the results for defects are very similar to those for spins: dynamic functions can be reduced to discretized overlaps and responses. Moreover we find FD plots made up of linear segments, as shown in Fig. 3. However, we find that the FDRs associated with the defects *differ quantitatively* from those of the spins, so we conclude that these numbers do not lead to useful effective temperatures.

These results are similar to those found for the East model [27]. However, the low temperature limits of the  $q_{nm}$  and  $x_{nm}$  can be estimated in the East model by rather simple arguments [43], whereas those in the TPM are more complex, and contain information about the mechanisms of relaxation in that system, as we now discuss. In the East model, relaxation from stage  $n - 1$  to stage  $n$  effectively consist of selecting a random set of excitations and removing them. This can be represented schematically by:

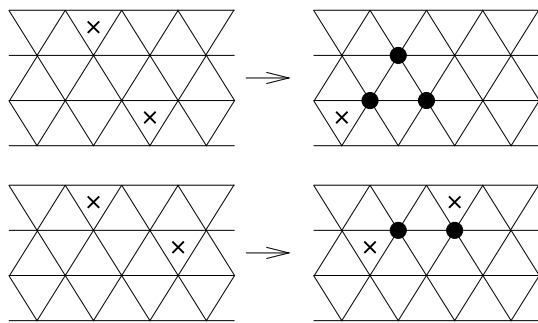


**Figure 4.** Processes in the TPM requiring an energy barrier of 1 unit. Spins are defined on the vertices of the lattice. The  $\times$  signs mark defects. The black dots show spins that must flip for a transition between the left and right states. (Top) Irreversible coagulation: a downward direction in the energy landscape. (Bottom) Reversible (‘diffusive’) event: the energy landscape is locally flat.

$$\begin{array}{cccccccccccc}
 1 & . & . & 1 & . & 1 & . & 1 & . & 1 & . & 1 & . & . & 1 & . & . \\
 1 & . & . & 1 & . & . & . & 1 & . & . & . & 1 & . & . & 1 & . & . \\
 1 & . & . & . & . & . & . & 1 & . & . & . & . & . & . & 1 & . & .
 \end{array}$$

where we show configurations of the East model’s defect variables, at three times, with the latest time at the bottom. Neighbouring defects in the first state are separated by gaps of length at least 1, so it representative of the first plateau. The second and third states are representative of the 2nd and 3rd plateaux respectively (gaps at least 2 and 4). We can see that

$$\langle n_i(t)n_i(t_w) \rangle \simeq \langle n_i(t) \rangle, \quad (17)$$

so that

$$q_{nm}^{(\text{East})} \simeq q_{nm}^{\max} \equiv \frac{1 - \langle n_i(t_w) \rangle}{1 - \langle n_i(t) \rangle}, \quad (18)$$

where  $t$  is a time within the  $n$ th plateau of  $c(t)$ , and  $t_w$  a time within the  $m$ th plateau.

In the TPM, the situation is different, since there are both reversible and irreversible moves taking place during the relaxation. Irreversible coagulation events involve removing two defects and adding a new one on a different site. Schematically, relaxation proceeds as:

$$\begin{array}{cccccccccccc}
 1 & . & . & 1 & . & . & 1 & . & . & 1 & . & 1 & . & . & 1 & . \\
 1 & . & . & . & 1 & . & . & . & . & 1 & . & . & . & 1 & . & .
 \end{array}$$

where pairs of defects combine to leave a single defect somewhere between the previous two. A more realistic representation of one such process is given in the top panel of Fig. 4. Additionally, reversible moves such as the one shown in the bottom panel of Fig. 4 can occur. In that particular example, two defects separated by distance 2 ‘rotate’ around a given plaquette. This process occurs on the same timescale as the coagulation event shown in the same figure. Both types of moves reduce the self and mutual overlaps of the plateau states. Numerically we confirm that  $q_{nm}^{\text{TPM}} < q_{nm}^{(\max)}$ , but we are not able to estimate  $q_{nm}^{\text{TPM}}$  analytically.

The second difference between the TPM and East models is that dynamics at low temperatures in the East model are those of irreversible events which allow no response, so that defect FDRs vanish as  $T \rightarrow 0$  [43]. In the TPM, the  $x_{nm}$  are finite numbers (except  $x_{n0} \simeq 0$ ); they become independent of temperature as  $T \rightarrow 0$ . The rate for ‘coagulation’ events is independent of the local field at low temperatures, but ‘diffusive’ events do allow a response. For instance, if we take the top left state of Fig. 4 as our initial condition, then we end in the top right one regardless of the local field: the response is zero. On the other hand, if we start in the bottom left state then the final state may be either the bottom left or bottom right one, with probabilities weighted by the local fields: the response is finite. In the energy landscape picture [9], ‘diffusive’ processes are along directions in which the energy landscape is flat, and ‘coagulative’ processes correspond to downward paths in the energy landscape. We conclude that  $x_{n,n-1}$  measures the relative rates for ‘diffusive’ and ‘coagulative’ events during the relaxation: a large value of  $x_{n,n-1}$  is a sign that ‘diffusive’ processes are dominating. We will confirm this statement explicitly for the SPM in section 3, since the relative rates for the two types of process can be controlled in that model.

Finally, we note that the field  $g_i$  is a local perturbation to the temperature; in the East model, this leads to negative FDRs, if the time  $t$  is between plateaux of  $c(t)$  [27, 43]. The same behaviour occurs in the TPM, but we consider only the plateau FDRs,  $x_{nm}$ , in this article. These quantities are positive (except for  $x_{n0} \simeq 0$ ).

### 2.3. Independent steps approximation

In the sketches of Fig. 2, we reduced the behaviour of local dynamic observables to a discrete set of numbers. We now show that if successive stages of the dynamics are statistically uncorrelated, then several relations between these numbers can be derived. These relations are satisfied by our numerical data.

We use only the fact that probabilities for combinations of independent events factorise. We define  $P_s(t, t')$  to be the probability that a defect survives on a given site from time  $t'$  to time  $t > t'$ . If relaxation proceeds by independent stages then we expect

$$P_s(t_n, t_m) = \prod_{n \geq n' > m} P_s(t_{n'}, t_{n'-1}), \quad (19)$$

where the times  $\{t_i\}$  separate the stages. We consider a situation where  $t_n$  is a time within the  $n$ th plateau.

A naive approximation for the survival probability would be to assume that  $P_s(t, t_w) \simeq \langle n_{it} n_{it_w} \rangle / \langle n_{it_w} \rangle$ , which is the probability that there is a defect on site  $i$  at time  $t$ , given that there was one on site  $i$  at time  $t_w$ . In the East model, this approximation is appropriate: we know that  $q_{nm} = q_{nm}^{\max}$ , and it follows that  $\langle n_{it_n} n_{it_m} \rangle \simeq \langle n_{it_m} \rangle \prod_{n'=m+1}^n \langle n_{it_{n'}} n_{it_{n'+1}} \rangle / \langle n_{it_{n'}} \rangle$ . On the other hand, the approximation fails if successive plateau states are completely uncorrelated, in which case  $\langle n_{it} n_{it_w} \rangle = \langle n_{it} \rangle \langle n_{it_w} \rangle$ . In this latter case, the naive approximation fails because it includes in the survival probability events in which the defect on site  $i$  is destroyed, and then replaced

**Table 1.** Mutual overlaps and FDRs in the TPM at  $\beta = 10$ . We test the predictions of Eqs. (22) and (25). Consistent with those equations, we find  $q_{31} \simeq q_{32}q_{21}$  and  $x_{21} \simeq x_{31}$ . We estimate the uncertainty for the spin overlaps to be less than 10% and those for the defect overlaps to be less than 20%; those for the FDRs are given. The (\*) indicates that the defect value of  $x_{31}$  was evaluated at  $t = 10^8$  (as in figure 3); the third stage of relaxation was not complete at this time, but the FDR still seems consistent with (25).

	$q_{21}$	$q_{32}$	$q_{31}$	$(q_{32}q_{21})$	$x_{21}$	$x_{31}$
Spins	0.63	0.43	0.26	(0.27)	$0.25 \pm 0.02$	$0.21 \pm 0.04$
Defects	0.25	0.053	0.009	(0.013)	$0.18 \pm 0.02$	$0.17 \pm 0.03(*)$

by a new defect. To take this into account, we estimate instead

$$P_s(t, t_w) \simeq \frac{\langle n_{it} n_{it_w} \rangle - \langle n_{it} \rangle \langle n_{it_w} \rangle}{\langle n_{it_w} \rangle (1 - \langle n_{it_w} \rangle)}. \quad (20)$$

With this approximation, the factorisation of probabilities for independent stages leads to

$$C_d(t, t_w) \simeq C_d(t, t_{n-1}) C_d(t_{n-1}, t_w), \quad (21)$$

which follows from (19) and (20), if the dynamics between times  $t_{n-1}$  and  $t$  are statistically uncorrelated with the dynamics between times  $t_w$  and  $t_{n-1}$ . Times  $t$  and  $t_w$  are chosen within the  $n$ th and  $m$ th stages, respectively. Correlators for spin observables factorise in a similar way. In terms of overlaps between plateau states, it follows that

$$q_{nm} = \prod_{n \geq n' > m} q_{n', n'-1}. \quad (22)$$

This relation is satisfied both for the East model and for completely uncorrelated stages. The dynamics of the TPM are rather slow, so that our data is limited, but we do obtain numerically that  $q_{31} \simeq q_{32}q_{21}$  for both the spin and defect autocorrelations, see Table 1.

To establish the effect of the independent stage approximation on the FDR, we consider the impulse response. In the presence of an instantaneous field  $h$  acting at time  $t_w$ , we expect the response to be given by the density of field-induced defects at stage  $n - 1$ , multiplied by the probability of these defects surviving to time  $t$ . That is,

$$\frac{d\langle n_i(t) \rangle_h}{dh} = P_s(t, t_{n-1}) \frac{d\langle n_i(t_{n-1}) \rangle_h}{dh}, \quad (23)$$

which holds if relaxation between  $t_{n-1}$  and  $t$  is independent of that between  $t_w$  and  $t_{n-1}$ , as before. The derivative of  $\chi(t, t_w)$  with respect to  $t_w$  is a response to an instantaneous field at  $t_w$ : taking care of normalisation, we find that

$$\left. \frac{\partial \chi_d(t, t_w)}{\partial t_w} \right|_t = C_d(t, t_{n-1}) \left. \frac{\partial \chi_d(t_{n-1}, t_w)}{\partial t_w} \right|_{t_{n-1}}. \quad (24)$$

Again, the analysis for spin observables is similar. Using the definition of the FDR, and Eq. (21), we arrive at  $X(t, t_w) = X(t_{n-1}, t_w)$ , and hence

$$x_{nm} = x_{n-1, m}, \quad (25)$$

for  $n - 1 > m$ . Thus,  $x_{nm}$  is a function of  $m$  only. The ‘self FDR’,  $x_{mm}$ , is close to unity. Physically, the FDR only depends on the stage of the dynamics during which the instantaneous field is applied. Our numerical results are again consistent with this analysis, see Table 1.

#### 2.4. Spatial structure in defect FDRs

In contrast to the spin degrees of freedom, defects have non-trivial spatial correlations in the TPM (except at equilibrium, where defect correlations vanish at equal times). Defining the Fourier transform of the plaquette field  $n_{\mathbf{k}}(t) = N^{-1/2} \sum_i n_i(t) e^{i\mathbf{k}\cdot\mathbf{r}_i}$ , where  $N$  is the number of plaquettes, we consider the correlator

$$\begin{aligned} \tilde{C}_d(k, t, t_w) &= \frac{\sum_{|\mathbf{k}'| \leq k} \langle n_{\mathbf{k}'}(t) n_{-\mathbf{k}'}(t_w) \rangle - \delta_{\mathbf{k}'} \langle n_{\mathbf{k}'} \rangle^2}{\sum_{|\mathbf{k}'| \leq k} (1)} \\ &= \frac{1}{N} \sum_{ij} F_k(|\mathbf{r}_i - \mathbf{r}_j|) [\langle n_i(t) n_j(t_w) \rangle - \langle n_i(t) \rangle \langle n_j(t_w) \rangle], \end{aligned} \quad (26)$$

where  $F_k(|\mathbf{r}|) = \frac{\sum_{|\mathbf{k}'| \leq k} e^{i\mathbf{k}'\cdot\mathbf{r}}}{\sum_{|\mathbf{k}'| \leq k} (1)}$  decays on a length scale of the order of  $k^{-1}$  from a value of unity at the origin. (Sums over wave vector  $\mathbf{k}$  are over the first Brillouin zone, with additional restrictions as specified.) Compared to the apparently simpler correlator  $\langle n_{\mathbf{k}}(t) n_{-\mathbf{k}}(t_w) \rangle$ ,  $\tilde{C}_d(k, t, t_w)$  attaches more weight to short distances; measurements of this quantity are therefore less affected by noise in the correlations at large distances. Moreover,  $\tilde{C}_d(k, t, t_w)$  interpolates smoothly between the local autocorrelation function when  $k$  is large, and the global correlation function of energy fluctuations at  $k = 0$ . Normalising as in the previous sections, we define

$$C_d(k, t, t_w) = \frac{\tilde{C}_d(k, t, t_w)}{\tilde{C}_d(k, t, t)} \quad (27)$$

We begin with the case  $t = t_w$ , which defines the static structure factor for the defects at time  $t_w$ :

$$S(k, t_w) \equiv \tilde{C}_d(k, t_w, t_w). \quad (28)$$

We plot this function in Fig. 5. We see that  $S(k, t_w)$  is an increasing function of  $k$ , which means that defects are surrounded by regions of reduced defect density. This is consistent with a local coagulative process which induces some effective repulsion between defects. There is a length scale associated with the  $k$ -dependence of  $S(k, t_w)$ : the time scale associated with coagulation of defects increases with their separation, so this length scale increases with  $t_w$ .

Moving to the time dependence of the correlation functions, we compare correlators at different wave vectors in the middle panel of Fig. 5. The plateau structure that is seen in the local correlations is not present at small  $k$ . Instead, the self overlaps of the plateau states approach unity, and the mutual overlaps approach zero. This is to be expected: within the plateau state, relaxation happens on small length scales, so fluctuations on large length scales do not relax, and self overlaps are large, for small  $k$ .

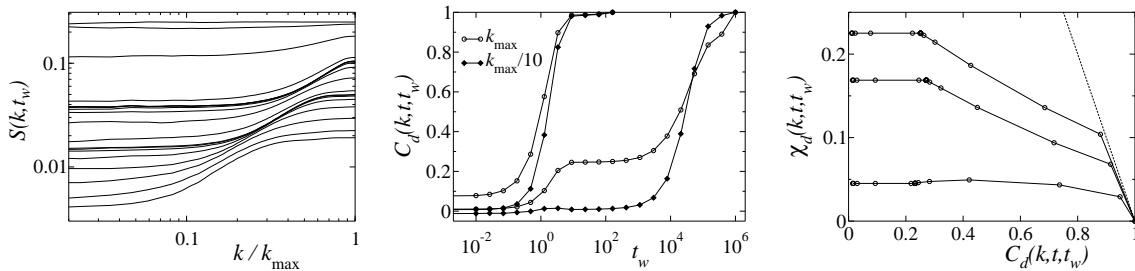


**Figure 5.** (Left) Structure factor of the defects,  $S(k, t_w)$ , at  $\beta = 10$ , and with  $t_w$  logarithmically spaced between  $10^{-2}$  and  $10^6$  (from top to bottom). A growing length scale is apparent, whose origin is the increasing range of coagulative events at large  $t_w$ . (Center) We show the correlation function of Eq. (26), for  $k \in \{k_{\max}, k_{\max}/10\}$ , where  $k_{\max}$  is the largest wave vector in the Brillouin zone. We have lowered the temperature to  $\beta = 20$ , and restrict ourselves to the first and second stages of relaxation. (Right) FD plots at  $\beta = 20$  for  $k \in \{k_{\max}, 2k_{\max}/3, k_{\max}/2\}$  (from top to bottom) showing decreasing response with decreasing  $k$ . The time is  $t = 2 \times 10^{10}$ ; at this temperature then this time is within the second plateau of  $c(t)$ .

On the other hand, successive plateau states do not retain any memory of the average density in the preceding plateau, so mutual overlaps at small  $k$  are very small.

The normalised response conjugate to  $C_d(k, t, t_w)$  is

$$\chi_d(k, t, t_w) = \frac{1}{C_d(k, t, t)} \frac{1}{N} \sum_{ij} F_k(|\mathbf{r}_i - \mathbf{r}_j|) \frac{d}{d(\beta g_j)} \langle n_i(t) \rangle. \quad (29)$$

It measures the response to a random field which is correlated over a length scale of  $k^{-1}$ . We present FD plots for three wave vectors in Fig. 5, at a single time  $t$  that is within the second plateau of  $c(t)$ . We find that the amplitude of the response functions quickly decrease when  $k$  decreases and vanish as  $k \rightarrow 0$ . This can be simply inferred from Fig. 1 since the energy density of each plateau states is temperature independent. Hence, the linear response of the energy to a temperature change vanishes in the small temperature limit. The situation is therefore similar to the one found in Ising or FA models [23, 27]:  $k$ -dependent FD plots smoothly interpolate from the one obtained from local autocorrelation functions to the one obtained for global quantities at  $k = 0$ , the crossover taking place when  $k\xi(t_w) \approx 1$ , where  $\xi(t_w)$  is a typical length scale characterizing the correlations between defects in the system.

### 3. Fluctuation-dissipation relations in the square plaquette model

#### 3.1. Early time regime: zero temperature dynamics

We now turn to the SPM, in which there are two relaxation stages. We begin our discussion with the initial stage, shown in the inset of Fig. 1. The corresponding FD plots for local spin and defect dynamic functions are shown in Fig. 6.

For the defect variables, we find that the self overlap within the plateau state is  $q_{11} \simeq 0.82$ . This number comes from isolated spins that can flip without energy

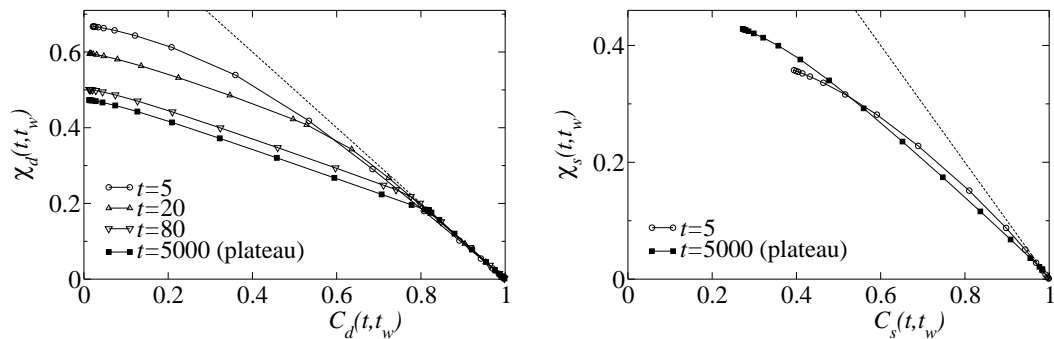


**Figure 6.** FD plots for the first stage of relaxation in the SPM at  $\beta = 20$ . We show the FDR for  $t = 5000$ , which is within the plateau of  $c(t)$ , and for several earlier times, at which the system is approaching the plateau. (Left) Defects, (right) spins. We show the equilibrium FDT with a dashed line.

penalty [5]. The mutual overlap between the plateau and initial states is very close to zero,  $q_{10} \simeq 0.01$ . A well-defined FDR can be determined,  $x_{10} \simeq 0.35$ , see Fig. 6. This makes the FD plot apparently very similar to the one found during the aging dynamics of mean-field spin glasses characterized by a one-step replica symmetry breaking transition at the static level [3, 5, 8].

For the spin degrees of freedom, we find  $q_{11} \simeq 0.98$  and  $x_{11} \simeq 1$ . For smaller correlation, however, the parametric FD plot is curved and there is no well-defined value for  $x_{10}$ .

This behaviour is qualitatively similar to that of the FA model, characterized by an initial “zero temperature” relaxation, followed by a reaction-diffusion aging regime. However, there are some important differences. Firstly, the decay into the initial plateau is exponential in the FA model, and the overlap  $q_{10}$  takes its maximal possible value  $q_{10} \simeq \frac{1-n_0}{1-n_{\text{plateau}}}$ , where  $n_{\text{plateau}}$  is the defect density in the plateau state, and  $n_0 = 1/2$  is the density in the initial state. This reflects the situation described by Eq. (18), in which the decay proceeds by uncorrelated relaxation events. Similarly, the FA model has  $x_{10} \rightarrow 0$  at low temperatures: this occurs because all Monte Carlo acceptance probabilities are either zero or unity at  $T = 0$ , and the dynamics are independent of the perturbing field; thus there is no response. On the other hand, the SPM has a finite value for  $x_{10}$  even at zero temperature, because there are energy conserving processes that have field-dependent acceptance probabilities close to  $1/2$ , even when  $T = 0$ .

We believe that the non-trivial zero temperature FDRs for both spins and defects come from the interplay between two types of process: reversible ‘diffusive’ spin flips in which the energy does not change, and irreversible ‘coagulative’ spin flips in which the energy is reduced. Both processes are occurring with similar rates. As discussed for the TPM, if the reversible process was dominating we would expect a large value for  $x_{10}$ , while irreversible relaxation would lead to a small value of  $x_{10}$ .

To confirm this analysis and probe in more detail the competition between diffusive and coagulative processes, we modify the Glauber dynamics, by introducing the

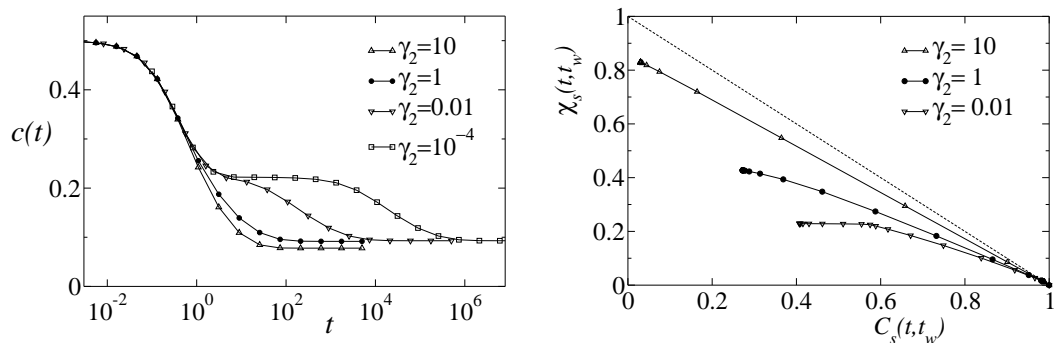


**Figure 7.** Correlation and response at  $T = 0$ , and their dependence on  $\gamma_2$ . (Left) Energy density  $c(t)$  (linear scale) after a quench to  $T = 0$ . Two stages are clearly visible at small  $\gamma_2$ ; at large  $\gamma_2$ , the extra energy-conserving processes allow more efficient exploration of configuration space, and the energy relaxes to a smaller value. (Right) Parametric plot for spin observables at the latest values of  $t$ . At small  $\gamma_2$ , the first stage of relaxation is purely ‘coagulative’ so it has  $x \simeq 0$ ; the second stage has both ‘diffusive’ and ‘coagulative’ processes, so  $x$  is finite. At large  $\gamma_2$ , energy-conserving (diffusive) processes dominate, and the FDR is large.

additional parameters  $\gamma$  in the rates of Eq. (A.1) (see Appendix A). Our aim is to affect the dynamics of the SPM in such a way that diffusive and coagulative processes become well-separated processes, in order to analyze the consequences for the resulting FD plots.

There are five types of move in the SPM: the energy change may be any of  $\pm 2, \pm 1, 0$ . We choose  $\gamma$  to depend on the modulus of the energy change and label these rates according to the number of defects adjacent to the spin that flips,  $u$ . This number satisfies  $u_{\text{final}} = 4 - u_{\text{initial}}$ , so we define three  $\gamma_{u_{\text{initial}}}$  factors for the three possible cases:

$$\begin{aligned} (u = 4) \leftrightarrow (u = 0) & \quad \text{multiplier } \gamma_4; \\ (u = 3) \leftrightarrow (u = 1) & \quad \text{multiplier } \gamma_3; \\ (u = 2) \leftrightarrow (u = 2) & \quad \text{multiplier } \gamma_2. \end{aligned}$$

The multipliers are the same for both forward and reverse processes, since the dynamics respect detailed balance. At zero temperature, the rates for the three forward processes are all independent and are given by  $(\gamma_4, \gamma_3, (\gamma_2/2))$ . We find that the behaviour depends only weakly on  $\gamma_4$  as long as  $\gamma_3 \geq \gamma_4$ . We therefore set  $\gamma_3 = \gamma_4 = 1$ , so that  $\gamma_2$  is a dimensionless measure of the rate for the energy-conserving, diffusive, events.

We show the energy decay and corresponding FD plots for spin observables in Fig. 7, as a function of  $\gamma_2$ . For  $\gamma_2 \ll 1$ , the zero temperature relaxation takes place in two stages, unlike the case of Fig. 1, in which  $\gamma_2 = 1$ . The first stage corresponds to pure coagulation: the system takes the path of steepest descent in the energy landscape. This process has an FDR of zero, as was the case for the first stage of relaxation in the TPM. In the second stage, the SPM explores its energy landscape by decreasing the energy where possible; otherwise, it makes energy-conserving moves. This stage has a finite FDR that reflects the ratio of energy-conserving, diffusive events (along flat directions



of the energy landscape) and coagulative events (along downward directions). We also note that this second stage is not a simple exponential decay, so the structure of Fig. 6 is not simply a result of two exponential relaxation mechanisms.

In the case  $\gamma_2 \gg 1$ , the increased rate for diffusive moves means that the system prefers to explore the energy landscape in directions along which the landscape is flat. It therefore explores more of configuration space, and is more likely to find pathways to low energy. Thus, the plateau state contains fewer defects than that for  $\gamma_2 = 1$ . Since the diffusive moves explore the constant energy surface in an unbiased way, the system tends to equilibrate locally between each coagulative move, and the FDR approaches unity as  $\gamma_2$  is increased.

Overall, we see that the finite value of  $x_{10}$  observed in Fig. 6 comes from competition between diffusive and coagulative processes. Its value,  $x_{10} \simeq 0.35$  for  $\gamma_2 = 1$  in fact depends continuously on the microscopic rates in the problem: we conclude that it is a non-universal number that measures the extent to which coagulation dominates over diffusion in the relaxational dynamics. In particular, the FDR has no connection with static quantities, in contrast to mean-field models [8, 12].

Moving to spatial structure, Eqs. (13, 14) also hold for the SPM, and spin correlation and response functions are independent of wave vector  $k$ . In the short time regime, the defect response is  $\mathcal{O}(k)$  at small  $k$ . This is because the zero temperature response comes only from energy-conserving processes, and the rates for these processes couple only to temperature gradients, and not to the absolute temperature. Our numerical simulations confirm that the response vanishes at small  $k$ . This was already demonstrated for the TPM in Fig. 5 so we do not show more data for the SPM.

### 3.2. Aging regime: activated dynamics

When the SPM is quenched to a small but finite temperature, the system eventually leaves the jammed state into which it relaxed initially, and enters an aging regime, in which the energy decays as a power law. We show local correlation-response data for both spins and defects in Fig. 8. As  $t$  and  $t_w$  get large, the local FDR approaches unity for all values of  $C$ , even though the system is still out of equilibrium.

In the framework of the previous sections, the approach of the FDR to unity comes from the fact that defects are very sparse at large  $t_w$ , and coagulation events become increasingly rare. The result is that diffusive processes dominate the response, and lead to  $X(q, t) \simeq 1$ , for finite  $q$  and large  $t$  [recall that  $X(q, t)$  is the FDR, evaluated at  $C(t, t_w) = q$ ; see (9)]. However, it is now a familiar feature of reaction-diffusion systems that there is structure in  $X(q, t)$  for finite  $t$  and small  $q$  [23, 27]. We define

$$X_\infty(t) = \lim_{q \rightarrow 0} X(q, t). \quad (30)$$

It was recently shown [27] that in the aging regime of the FA model,  $X_\infty(t)$  is a negative number that depends on the dimension of the system, but not on the time  $t$ . Observables associated with domain walls in the Glauber-Ising chain have similar behaviour, with

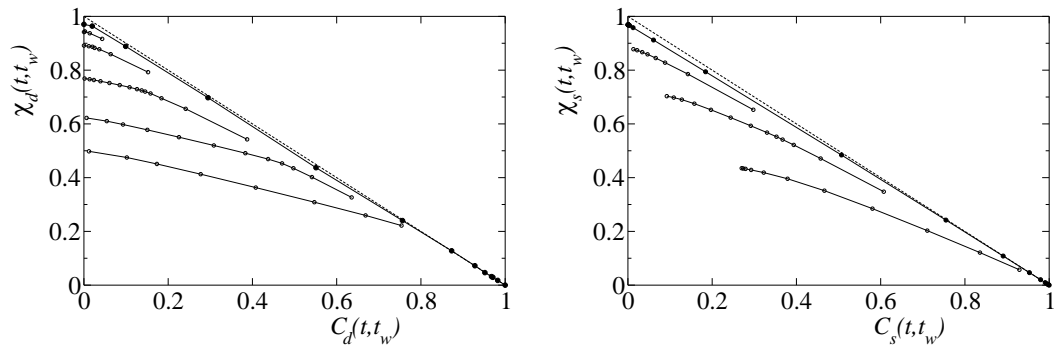


**Figure 8.** Correlation and response in the aging regime for the SPM. (Left) Defects: we show  $t \in \{140, 2500, 1.0 \times 10^4, 4.3 \times 10^4, 1.8 \times 10^5, 7.4 \times 10^5\}$ , which decrease from top to bottom. (Right) Spins: final times are  $t \in \{140, 1.6 \times 10^4, 1.1 \times 10^5, 7.4 \times 10^5\}$ , with the same trend. For both cases, the first time is representative of the initial plateau in  $c(t)$ : recall Fig. 6. Except for the latest time, we concentrate on the region in which equilibrium FDT is not obeyed; the parametric plot goes through  $(C, \chi) = (1, 0)$ , for all values of  $t$ , but we do not plot data in this region.

$X_\infty = 0$  [23]. However, for both these models,  $X(q, t)$  only converges to its limiting value at very small  $q$ . This requirement also necessitates working at large  $t$ : the limit of long times and very small  $q$  makes direct investigation of this limit very difficult in simulations. For the FA model and the Glauber-Ising chain,  $X_\infty$  is independent of the observation wave vector,  $k$ . From the point of view of simulations, it is fortunate that  $X_\infty$  is typically much easier to measure at small wave vector.

In Fig. 9, we show that the spatial structure of defect correlation and response in the SPM is consistent with this behaviour. That is,  $X(q, t)$  is positive and close to unity for large  $q$ , and negative for small  $q$ . The value of  $q$  at which the crossover takes place depends on the observation wave vector  $k$ ; its value is close to unity at large  $k$  and close to zero at small  $k$ . The physical origin of a negative asymptotic FDR is the same as for the FA and East models [27]: when applying a small temperature change  $\delta T > 0$ , ( $T$  is the field conjugate to the energy), the dynamics of the system gets accelerated and the energy decays faster towards equilibrium so that  $\delta c(t) < 0$ , and indeed  $\delta c(t)/\delta T < 0$ , unlike the equilibrium case.

We now discuss how the limiting negative value of the FDR and the overall behaviour observed in fig. 9 can be predicted by a similar calculation to that used for the FA model in Ref. [27]. The calculation for the SPM is slightly more involved, due to the presence of two growing length scales in the aging regime of that model. As discussed in [6], the reaction-diffusion dynamics involve exchange of defect dimers between isolated single defects. This process takes place over a length scale  $\ell(t) \sim [1/n_i(t)]$ ; at long times then this length scale is much larger than the correlation length for density fluctuations in the aging regime, which is  $\xi(t) \sim [1/n_i(t)]^{1/2}$ . The processes by which dimers are exchanged have an energy barrier of two. Their rates are also inversely proportional to the distance  $\ell(t)$  over which the dimer must travel [5, 6]. The result is that these rates depend linearly on the defect density in the system, averaged over a region of linear

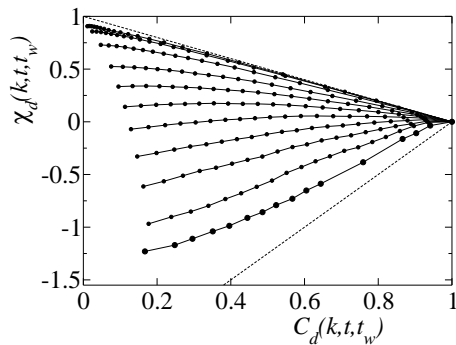


**Figure 9.** Parametric FD plot for spatially dependent defect observables at  $\beta = 5$  and  $t = 7.4 \times 10^4$  (this time is within the aging regime). The wave vectors are  $k/k_{\max} \in \{1.0, 0.50, 0.33, 0.24, 0.20, 0.17, 0.14, 0.11, 0.083, 0.050, 0.0\}$ , with  $k$  decreasing from top to bottom. Dashed lines show the equilibrium FD relation, and the small  $k$  prediction of (B.29). The deviations from the small  $k$  prediction arise from corrections to the aging limit, as discussed in the main text and in Fig. 10. The response at  $k = 0$  was calculated using an explicit field, rather than the no-field method described in Appendix A, since that method is rather inefficient for responses at small  $k$ .

extent  $\ell(t)$ .

In Appendix B, we show how this situation can be described by an effective reaction-diffusion system, where correlations in the aging regime can be calculated in a field-theoretic formalism. The rates for reaction and diffusion depend the density, averaged over a region of fixed size  $\ell$ . We neglect the time dependence of this length scale, but our results depend only on whether  $k\ell$  is large or small compared to unity. Hence, our results apply if  $k\ell(t_w)$  and  $k\ell(t)$  are both small, or both large. The other parameter that enters the FDR is  $z_k(t_w) = Dk^2/[2\lambda n(t_w)]$ , which measures the relative size of  $k$  and  $\xi(t)$ .

The calculation described in Appendix B is quite lengthy, but the important result is (B.29). At small  $k$ , the FD plot is a straight line with gradient  $X = -(5/2)$ . At large  $k$ , we expect quasi-equilibrium behaviour,  $X = 1$  (reversible ‘diffusive’ processes dominate on small length scales). Further, we can identify an intermediate regime, in which  $k\ell(t)$  and  $k\ell(t_w)$  are both large, but  $k\xi(t)$  and  $k\xi(t_w)$  are both small. We find that this regime has  $X = -3$ .

Comparing with the results of figure 9, the behaviour is in qualitative agreement with the field theoretic calculation. However, quantitative agreement is rather poor for the limit of small wave vector, and the intermediate regime is not apparent. To understand this, we observe that the field theoretic calculation is valid only deep in the aging regime, which requires

$$\langle n_i(t_w) \rangle, \langle n_i(t) \rangle \ll 1, \quad \langle n_i(t) \rangle \gg e^{-\beta} \quad (31)$$

We also predict logarithmic corrections to these tree level results, since the critical dimension of the reaction-diffusion system is  $d_c = 2$  (to show this, one must be careful to take  $n(t)\ell(t)^2$  to infinity, in the limit of large time).

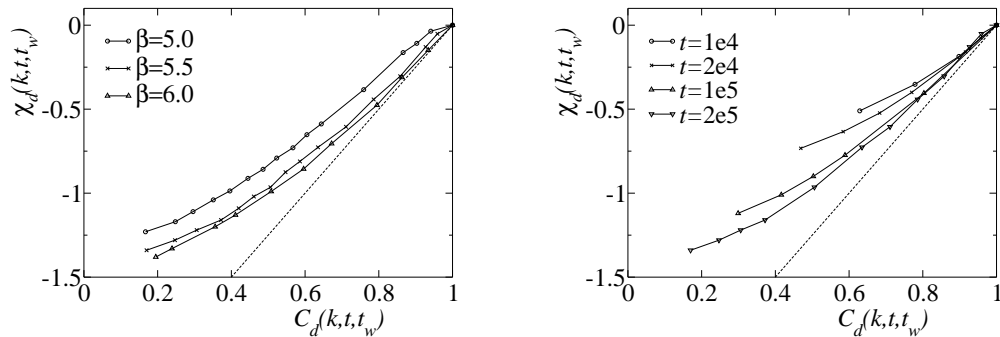


**Figure 10.** Parametric FD plots in the SPM at  $k = 0$ . As the bounds of (31) are improved, the data approaches the prediction  $X = -(5/2)$ , which is shown as a dashed line. (Left) Increasing  $\beta$  with a constant value of the rescaled time ( $c^2t = 3.3$ ) improves the bound  $\langle n_i(t) \rangle \gg e^{-\beta}$ . This improves the agreement with theory for  $t_w$  close to  $t$ . (Right) Increasing  $t$  and  $t_w$  at fixed temperature improves the bound  $\langle n_i(t_w) \rangle \ll 1$ , which increases the range over which the system is close to the prediction for the aging limit.

The conditions of (31) are rather restrictive, necessitating simulations at low temperatures and long times. While we were not able to access the regime of intermediate  $k$ , we show in figure 10 that the FDR at  $k = 0$  does appear to approach  $-(5/2)$  as we improve the bounds of (31). Our data is therefore consistent with a value of  $X_\infty = -(5/2)$ , although convergence to this limit is rather slow.

#### 4. Conclusion

Finally, we bring together the results of the previous sections and discuss their significance. We have shown that the FDR in these plaquette models has considerable structure. By using the ‘no-field’ method of Refs. [38, 39], we have been able to perform systematic measurements of correlation-response relations allowing resolution of the questions about the SPM and TPM that were raised in Refs. [5, 21].

By definition, the FDR measures the ability of a system to respond to an external perturbation (normalised by an equilibrium system with the same correlations). We have argued throughout that when the temperature is small, the system can only respond by ‘diffusive’ energy-conserving processes. A large FDR means that these processes are dominating (for example, this occurs in dilute reaction-diffusion systems); a small FDR means that irreversible ‘coagulative’ processes are dominating (for example, the East model). This is consistent with our interpretation of the FDR as a purely dynamic object in these systems, which have a single pure state at all finite temperatures. It contrasts with the situation following a quench into a regime in which ergodicity is broken, where the long time limit of the FDR should reflect the underlying pure state structure [8, 12].

We have shown in particular that the multi-stage relaxation of the plaquette models leads to well-defined FDRs within each stage, with values ranging from  $X = 1$  for quasi-

equilibrium regimes, non-trivial  $0 < X < 1$  for local observables within activated stages, and non-trivial  $X < 0$  for global observables coupled to thermal activation. Therefore, plaquette models present an extremely rich aging behaviour that should be considered as an alternative paradigm to mean-field models when interpreting numerical data on physical systems such as disordered magnets or supercooled liquids.

## Acknowledgments

We thank Peter Mayer and Peter Sollich for useful discussions. This work was supported by NSF grant CHE-0543158 (RLJ); by EPSRC grants GR/R83712/01 (RLJ and JPG) and GR/S54074/01 (JPG); and by University of Nottingham grant no. FEF 3024 (JPG).

## Appendix A. Measuring response functions

In this Appendix we give the generalisation of the ‘no-field’ method of [38, 39] to continuous time processes: we used this method to calculate all responses to local fields in this article.

Suppose that we have a spin system with Hamiltonian  $H = H_0 - \sum_i h_i s_i$ , where  $s_i \in \{-1, 1\}$ ; the sum is over all the spins, and the  $h_i$  are time-dependent local fields. We choose a continuous time dynamics that obeys detailed balance, in which the spin on site  $i$  flips with a rate

$$W_i = \frac{\gamma_i}{1 + \exp[\beta(\Delta_i + 2h_i s_i)]}, \quad (\text{A.1})$$

where  $\beta$  is the inverse temperature;  $\Delta_i$  is the change in  $H_0$  on flipping spin  $i$ ; and  $\gamma_i$  is a local rate that does not depend on the state of spin  $i$  or on the field  $h_i$ . Glauber dynamics is the case when  $\gamma_i = 1$  throughout. In kinetically constrained models, we have  $\gamma_i \in \{0, 1\}$  according to state of the neighbours of spin  $i$ . In section 3.1, we consider a modified Glauber dynamics, such that  $\gamma_i$  depends on the environment of each spin. However, the local field  $h_i$  always couples to the dynamics as in (A.1).

The application the method of [38, 39] to this continuous time system is as follows: the integrated response of observable  $A$  to the field  $h_i$  is

$$\chi_i^{(A)}(t, t_w) \equiv \left. \frac{d\langle A(t) \rangle}{d(\beta h_i)} \right|_{h_i=0} = \langle A(t) \mathcal{R}_i(t, t_w) \rangle_{h_i=0} \quad (\text{A.2})$$

where the field  $h_i$  acts on site  $i$  between the times  $t_w$  and  $t$ , and

$$\mathcal{R}_i(t, t_w) = \sum_{\text{flips} \in (t_w, t)} \frac{-2s_{i, t_{\text{flip}}^-}}{1 + \exp(-\beta \Delta_{i, t_{\text{flip}}^-})} + \int_{t_w}^t dt' \frac{2s_{it'} \gamma_{it'} \exp(\beta \Delta_{it'})}{[1 + \exp(\beta \Delta_{it'})]^2}, \quad (\text{A.3})$$

where the sum is over the flips of spin  $i$  within the given time window; the notation  $t_{\text{flip}}^-$  indicates that the summand is to be evaluated just before the spin flip. The strength of this method is that the small field  $h_i$  does not enter (A.3).

We now outline a derivation of (A.3). Let a trajectory be a sequence of configurations of the system at a series of time steps, where sequential configurations differ in at most one spin. The probability of a given trajectory is given by

$$P_{\text{traj}} = \left[ \prod_{\tau=1}^{t/\epsilon} W_{\mathcal{C}_\tau, \mathcal{C}_{\tau-1}} \right] p_0(\mathcal{C}_0), \quad (\text{A.4})$$

where  $\mathcal{C}_\tau$  represents the state of the whole system in the  $\tau$ th configuration;  $p_0(\mathcal{C}_0)$  is the probability of the initial condition;  $\epsilon$  is the microscopic time step; and

$$W_{\mathcal{C}', \mathcal{C}} = \delta_{\mathcal{C}', \mathcal{C}} \left( 1 - \epsilon \sum_i W_i \right) + \epsilon \sum_i \delta_{s_i + s'_i} W_i \quad (\text{A.5})$$

is the probability of a transition from state  $\mathcal{C}$  to state  $\mathcal{C}'$ , in a time  $\epsilon$ . We use  $s_i$  (or  $s'_i$ ) to denote the state of spin  $i$  in configuration  $\mathcal{C}$  (or  $\mathcal{C}'$ ); the rates  $W_i$  are defined in (A.1).

We note that the microscopic time step must be small enough to ensure that  $W_{\mathcal{C}', \mathcal{C}}$  is always positive. Simple discrete time Monte Carlo dynamics have  $W_i \leq 1$  for all  $i$ , and  $\epsilon = N^{-1}$  where  $N$  is the total number of spins. Here we explicitly allow for  $\epsilon < N^{-1}$  since we wish to take the continuous time limit. Also, recall that  $P_{\text{traj}}$  is defined only for trajectories in which successive configurations differ in at most one spin. Thus we have  $\sum_{\mathcal{C}'} W_{\mathcal{C}', \mathcal{C}} = 1$ , as long as the sum is taken over states  $\mathcal{C}'$  that differ from  $\mathcal{C}$  in at most spin; this ensures conservation of probability.

The definition of the stochastic average is then

$$\langle A \rangle = \sum_{\text{traj}} A_{\text{traj}} P_{\text{traj}}, \quad (\text{A.6})$$

where  $A_{\text{traj}}$  is the value of the observable  $A$  for the given trajectory, and the sum is over all possible trajectories.

To calculate the integrated response, we simply write

$$\begin{aligned} \frac{d}{d(\beta h_i)} P_{\text{traj}} &= \sum_{\tau'=(t_w/\epsilon)+1}^{t/\epsilon} \left[ \prod_{\tau=\tau'+1}^{t/\epsilon} W_{\mathcal{C}_\tau, \mathcal{C}_{\tau-1}} \right] \times \\ &\quad \left[ \frac{d}{d(\beta h_i)} W_{\mathcal{C}_{\tau'}, \mathcal{C}_{\tau'-1}} \right] \left[ \prod_{\tau=1}^{\tau'-1} W_{\mathcal{C}_\tau, \mathcal{C}_{\tau-1}} \right] p_0(\mathcal{C}_0), \end{aligned} \quad (\text{A.7})$$

where we assumed that the field acted only between times  $t_w$  and  $t$ , as before. We then write  $[dW_{\mathcal{C}'\mathcal{C}}/d(\beta h_i)] = R_{\mathcal{C}'\mathcal{C}} W_{\mathcal{C}'\mathcal{C}}$ , which defines the matrix elements  $R_{\mathcal{C}'\mathcal{C}}$  (at least for  $W_{\mathcal{C}'\mathcal{C}} > 0$ , which is the only relevant case). Hence,

$$\frac{d}{d(\beta h_i)} \langle A \rangle = \sum_{\text{traj}} A_{\text{traj}} P_{\text{traj}} \sum_{\tau=t_w/\epsilon}^{t/\epsilon} R_{\mathcal{C}_\tau, \mathcal{C}_{\tau-1}}. \quad (\text{A.8})$$

Explicitly constructing the matrix  $R_{\mathcal{C}_\tau, \mathcal{C}_{\tau-1}}$  as in Ref. [38], and then taking the limit of continuous time,  $\epsilon \rightarrow 0$ , leads to (A.3).

To calculate the defect response in the plaquette models, we also require the response for cases where the random field couples not to a single spin, but to a local function of several spins. For example, consider the response to a perturbation

$$\delta H = -g_i s_1 s_2 s_3 s_4 \equiv -g_i n_i$$

where the second equality defines the dual plaquette variable  $n_i$ . In that case,

$$\frac{d}{d(\beta g_i)} \langle A(t) \rangle = \langle A(t) \mathcal{S}_i(t, t_w) \rangle \quad (\text{A.9})$$

where the perturbation acts between times  $t_w$  and  $t$  as before, and

$$\mathcal{S}_i(t, t_w) = \sum_{a \in \{1,2,3,4\}} \left\{ \sum_{\text{flips} \in (t_w, t)} \frac{-2n_{i, t_{\text{flip}}}^-}{1 + \exp(-\beta \Delta_{a, t_{\text{flip}}}^-)} + \int_{t_w}^t dt' \frac{2n_{i, t'} \gamma_{at'} \exp(\beta \Delta_{at'})}{[1 + \exp(\beta \Delta_{at'})]^2} \right\}. \quad (\text{A.10})$$

The sum inside the curly brackets is over flips of spin  $a$ , and the summand is again evaluated just before the spin flip.

## Appendix B. Field theory for defects in the SPM

In this appendix, we define an effective reaction-diffusion system that takes account of the two growing length scales in the aging regime of the SPM. We calculate that correlation and response in this system at tree-level, following [46]. The methods are quite standard, so we quote only the main results; the review of [47] gives technical details of this formalism.

### Appendix B.1. Effective theory and dynamical action

The effective theory is defined for defects on a cubic lattice of  $N$  sites in  $d$  dimensions, with integer occupancy on each site. Diffusion takes place between neighbouring sites, and annihilation takes place on a single site. That is,

$$\begin{aligned} n_i n_j &\rightarrow (n_i - 1), (n_j + 1), & \text{rate } n_i D_{ij} \\ n_i &\rightarrow (n_i - 2), & \text{rate } n_i (n_i - 1) \lambda_i. \end{aligned} \quad (\text{B.1})$$

The rates  $D_{ij}$  and  $\lambda_i$  depend on the local defect density. We also require their coupling to perturbations to the energy and to the inverse temperature  $\beta$ . We write the energy as  $E = \sum_i n_i - \sum_i h_i n_i$ , and the appropriate rates are

$$D_{ij} = 2D_0 \frac{e^{-\beta(2-h_i-h_j)}}{1 + e^{\beta(h_i-h_j)}} \sum_{i'} g_{i';ij}^{(D)} n_{i'} \quad (\text{B.2})$$

$$\lambda_i = \lambda_0 e^{-2\beta(1-h_i)} \sum_{i'} g_{i';i}^{(\lambda)} n_{i'}. \quad (\text{B.3})$$

Both rates are of activated form, with energy barriers close to two, since they require an intermediate stage containing a dimer. The factor  $e^{\beta(h_i-h_j)}$  in the denominator of  $D_{ij}$

sets the coupling to the random potential  $h$ . The functions  $g_{i';ij}^{(D)}$  and  $g_{i';i}^{(\lambda)}$  decay with the distance between sites  $i$  and  $i'$ , on a length scale  $\ell$ . They vanish at  $i' = i$  and  $i' = j$ , and  $g_{i';ij}^{(D)}$  is symmetric in  $i$  and  $j$ . We also normalise such that  $\sum_{i'} g_{i';ij}^{(D)} = \sum_{i'} g_{i';i}^{(\lambda)} = 1$ .

The master equation for this system can be written in an operator formalism [48]. We introduce a bosonic algebra:  $[a_i, a_j] = [a_i^\dagger, a_j^\dagger] = 0$ ;  $[a_i, a_j^\dagger] = \delta_{ij}$ , and a vacuum state  $|0\rangle$ , such that  $a_i|0\rangle = 0$ , for all  $i$ . Let the probability of a configuration  $\{n_i\}$  be  $P(\{n_i\})$ , and let  $|P(t)\rangle = \sum_{\{n_i\}} P(\{n_i\}, t) \prod_i (a_i^\dagger)^{n_i} |0\rangle$ . Then the master equation is

$$\partial_t |P(t)\rangle = -\hat{W}|P(t)\rangle \quad (\text{B.4})$$

with

$$\begin{aligned} \hat{W} = & \sum_{\langle ij \rangle} (1/2)(a_i^\dagger - a_j^\dagger)[(\hat{D}_{ij} + \hat{D}_{ji})(a_i - a_j) + (\hat{D}_{ij} - \hat{D}_{ji})(a_i + a_j)] \\ & + \sum_i \hat{\lambda}_i [(a_i^\dagger)^2 - 1] a_i^2 \end{aligned} \quad (\text{B.5})$$

where  $\hat{D}_{ij}$  and  $\hat{\lambda}_i$  are now operators, since they depend on the densities  $n_{i'} = a_{i'}^\dagger a_{i'}$ .

We now construct a path integral representation of the dynamics. We work in the coherent state representation, in which operators have matrix elements  $O(\phi, \bar{\phi}) = \langle 0 | e^{\sum_i (\bar{\phi}_i + 1) a_i} \hat{O} e^{-\sum_i \phi_i a_i^\dagger} | 0 \rangle e^{-\sum_i (\bar{\phi}_i + 1) \phi_i}$ . We take the continuum limit, denoting the lattice spacing by  $l_0$ , and the position of site  $i$  by  $\mathbf{r}_i$ ; we define  $\phi(\mathbf{r}) = \sum_i \phi_i \delta(\mathbf{r} - \mathbf{r}_i)$  and  $\bar{\phi}(\mathbf{r}) = (l_0)^d \sum_i \bar{\phi}_i \delta(\mathbf{r} - \mathbf{r}_i)$ , so that the dimensions of the field  $\phi(\mathbf{r}, t)$  are those of density, and  $\bar{\phi}(\mathbf{r}, t)$  is dimensionless. In a similar way, the field  $h(\mathbf{r}, t) = (l_0)^d \sum_i h_i \delta(\mathbf{r} - \mathbf{r}_i)$  has dimensions of energy. The local density of excitations is

$$\rho(\mathbf{r}, t) = [1 + \bar{\phi}(\mathbf{r}, t)] \phi(\mathbf{r}, t). \quad (\text{B.6})$$

We also define  $g(\mathbf{r}) = g_{i';i} \delta[\mathbf{r} - (\mathbf{r}_{i'} - \mathbf{r}_i)]$  and we choose  $g_{i';ij}$  to have the same spatial dependence:  $g_{i';ij} = g[\mathbf{r}_{i'} - (1/2)(\mathbf{r}_i + \mathbf{r}_j)]$ .

Finally, the path integral representation of the generating function for the dynamics is  $Z = 1 = \int \mathcal{D}[\phi, \bar{\phi}] \exp(-S[\phi, \bar{\phi}])$ , with

$$S[\phi, \bar{\phi}] = \int dt d^d \mathbf{r} \bar{\phi}(\mathbf{r}, t) \partial_t \phi(\mathbf{r}, t) + \int dt H[\phi, \bar{\phi}, t] \quad (\text{B.7})$$

where

$$\begin{aligned} H[\phi, \bar{\phi}, t] = & \int d^d \mathbf{r} d^d \mathbf{r}' g(\mathbf{r} - \mathbf{r}') [1 + \bar{\phi}(\mathbf{r}', t)] \phi(\mathbf{r}', t) \times \\ & \left\{ D \nabla \bar{\phi}(\mathbf{r}, t) \cdot [(1 + 2\beta h(\mathbf{r}, t)) \nabla \phi(\mathbf{r}, t) - \phi(\mathbf{r}, t) \beta \nabla h(\mathbf{r}, t)] \right. \\ & + \lambda \bar{\phi}(\mathbf{r}, t) [2 + \bar{\phi}(\mathbf{r}, t)] [1 + 2\beta h(\mathbf{r}, t)] \phi(\mathbf{r}, t)^2 \\ & \left. + \mathcal{O}(\nabla^4, h^2) \right\} \end{aligned} \quad (\text{B.8})$$

and  $\lambda = \lambda_0 l_0^{2d}$ ,  $D = D_0 l_0^{2+d}$

We work to linear order in the perturbation  $h$  and to quadratic order in a gradient expansion; we also neglect boundary contributions to the action.

This concludes our definition of the effective theory. We now calculate the time dependence of the density, and the propagator in the system.



## Appendix B.2. Mean density and propagator

For the calculations of this subsection, we set the perturbing field  $h = 0$ . This field only enters the calculation of the response, in the next subsection. To calculate the average density, we write

$$\partial_t n(t) \equiv \partial_t \langle \rho(\mathbf{r}, t) \rangle = \langle \partial_t \phi(\mathbf{r}, t) \rangle. \quad (\text{B.9})$$

where the average is over trajectories with initial density  $n_0$ , and weights given by the action of (B.7).

Transforming to momentum space, we define  $\phi_{\mathbf{k}}(t) = \int d^d \mathbf{r} e^{i\mathbf{k} \cdot \mathbf{r}} \phi(\mathbf{r}, t)$ , and similarly  $\bar{\phi}_{\mathbf{k}}(t)$ . The Fourier transform of  $g(\mathbf{r})$  depends only on  $k = |\mathbf{k}|$  and is denoted by  $g_k$ . Working at tree level, we evaluate  $\langle \partial_t \phi(\mathbf{r}, t) \rangle$  at the saddle point, whose position is given by the Euler-Lagrange equation  $\delta S / \delta \bar{\phi}_{-\mathbf{q}}(t) = 0$ . Writing out this equation for  $q = 0$ , we arrive at

$$\langle \partial_t \phi_{q=0}(t) \rangle = -\lambda \int d^d \mathbf{r} d^d \mathbf{r}' g(\mathbf{r}' - \mathbf{r}) \left\langle A[\bar{\phi}(t)] \phi(\mathbf{r}, t)^2 \phi(\mathbf{r}', t) \right\rangle \quad (\text{B.10})$$

where  $A[\bar{\phi}(t)]$  is a function that depends on all of the Fourier components of  $\bar{\phi}$ , evaluated at a single time  $t$ . To evaluate the right hand side of (B.10), we note that all expectation values of the form  $\langle \bar{\phi}(t) B[\phi(t)] \rangle$  vanish (where  $B[\phi(t)]$  again denotes a function that is local in time but depends on all Fourier components of the field  $\phi$ ). Further, the tree level approximation is that  $\langle B[\phi(t)] \rangle = B[\langle \phi(t) \rangle]$  for any function  $B$ . Hence, we arrive at

$$\partial_t n(t) = -2\lambda n(t)^3, \quad (\text{B.11})$$

where we used the fact that  $g_{k=0}$  is normalised to unity, and  $A[\bar{\phi} = 0] = 2$ . Starting from an initial condition with density  $n_0$ , we arrive at the mean density:

$$n(t) = \frac{n_0}{\sqrt{1 + 4\lambda n_0^2 t}}, \quad (\text{B.12})$$

We now calculate the propagator for the dynamics, defined by

$$G_k(t, w) = (Nl_0^d)^{-1} \langle \phi_{\mathbf{k}}(t) \bar{\phi}_{-\mathbf{k}}(w) \rangle, \quad (\text{B.13})$$

which satisfies  $\lim_{w \rightarrow t^-} G_k(t, w) = 1$ . To calculate the time dependence of  $G_k(t, w)$ , we obtain the time derivative of  $\bar{\phi}_{-\mathbf{k}}(t)$  from a second Euler-Lagrange equation,  $\delta S / \delta \phi_{\mathbf{k}}(t) = 0$ . At tree level, the only non-vanishing contributions to  $\langle \phi_{\mathbf{k}}(t) \partial_w \bar{\phi}_{-\mathbf{k}}(w) \rangle$  are of the form

$$\langle \phi_{\mathbf{k}}(t) \bar{\phi}_{-\mathbf{k}}(w) U_k[\phi(w)] \rangle. \quad (\text{B.14})$$

(Terms of the form  $\langle \phi_{\mathbf{k}}(t) \bar{\phi}_{-\mathbf{k}}(w) \bar{\phi}_{-\mathbf{k}'}(w) U_k'[\phi(w)] \rangle$  vanish since every field  $\bar{\phi}$  must be contracted with a field  $\phi$  at a later time.) Making the only possible contraction, and evaluating the function  $U_k[\phi(w)]$  at the saddle point, we arrive at

$$\partial_w G_k(t, w) = G_k(t, w) U_k[\langle \phi(w) \rangle] \quad (\text{B.15})$$

Finally, we use the Euler-Lagrange equation to identify  $U_k[\langle\phi(w)\rangle] = Dk^2n(w) + 2\lambda(2 + g_k)n(w)^2$ . Hence:

$$G_k(t, w) = \left(\frac{n(t)}{n(w)}\right)^{2+g_k} e^{z_k(w)-z_k(t)}, \quad (\text{B.16})$$

with

$$z_k(t) = Dk^2/[2\lambda n(t)] \quad (\text{B.17})$$

Armed with expressions for  $n(t)$  and  $G_k(t, w)$  we are now in a position to calculate the correlation and response.

### Appendix B.3. Correlation and response

The two-point defect correlation function analogous to  $\tilde{C}_d(k, t, t_w)$  is

$$C_\phi(k, t, t_w) \equiv \int d^d\mathbf{r} e^{i\mathbf{k}\cdot\mathbf{r}} [\langle\rho(\mathbf{r}, t)\rho(\mathbf{0}, t_w)\rangle - n(t)n(t_w)]. \quad (\text{B.18})$$

The integrand decomposes as

$$e^{i\mathbf{k}\cdot\mathbf{r}} [\langle\phi(\mathbf{r}, t)\bar{\phi}(\mathbf{0}, t_w)\phi(\mathbf{0}, t_w)\rangle + \langle\delta\phi(\mathbf{r}, t)\delta\phi(\mathbf{0}, t_w)\rangle], \quad (\text{B.19})$$

where  $\delta\phi(\mathbf{r}, t) = \phi(\mathbf{r}, t) - n(t)$ . This correlation is to be evaluated at  $h = 0$ .

At tree level, the integral of the first term of (B.19) is simply  $[G_k(t, t_w)n(t_w)]$ . We can evaluate the second term by direct consideration of its equations of motion. However, it is simpler to identify the tree level contributions to this quantity directly: expanding the time-ordered exponential  $e^{-S}$ , the only terms contributing at tree-level come from:

$$\left\langle\delta\phi(\mathbf{r}, t)\delta\phi(\mathbf{r}', t_w) \int_0^{t_w} ds H[\phi, \bar{\phi}, s]\right\rangle. \quad (\text{B.20})$$

This expectation value can be calculated straightforwardly, by making the allowed contractions and using the tree level relation  $\langle B[\phi(s)]\rangle = B[\langle\phi(s)\rangle]$ . The result is that

$$\langle\delta\phi_{-\mathbf{k}}(t)\delta\phi_{\mathbf{k}}(w)\rangle = -2\lambda(Nl_0^d) \int_0^w ds G_k(t, s)G_k(w, s)n(s)^3(1 + 2g_k) \quad (\text{B.21})$$

Making the change of variables,  $z_s = Dk^2/[2\lambda n(s)]$ , leads to

$$\langle\delta\phi_{-\mathbf{k}}(t)\delta\phi_{\mathbf{k}}(w)\rangle = - (Nl_0^d)n(w)G_k(t, w)z_w^{-3-2g_k} \times \int_{z_0}^{z_w} dz_s (1 + 2g_k)z_s^{2+2g_k} e^{2z_s-2z_w} \quad (\text{B.22})$$

This tree level calculation is valid in the aging regime, when  $n(t_w) \ll n(t = 0)$ . In this limit, the integrand is dominated by large  $z_s$ , and the behaviour is independent of the initial condition. We therefore evaluate the correlation at  $z_0 = 0$ .

The regimes of interest are  $k\ell \gg 1$ , for which  $g_k \simeq 0$ , and  $k\ell \ll 1$  for which  $g_k \simeq 1$ . The integral can be performed in these limits. Bringing everything together, we arrive at

$$C_\phi(k, t, t_w) = n(t_w)G_k(t, t_w)F[z_k(t_w), g_k] \quad (\text{B.23})$$

where  $z_k(t)$  was defined in (B.17), and

$$F[z, 0] = 1 - (1/4)[2z^{-1} - 2z^{-2} + z^{-3}(1 - e^{-2z})] \quad (\text{B.24})$$

$$F[z, 1] = 1 - (3/4)[2z^{-1} - 4z^{-2} + 6z^{-3} - 6z^{-4} + 3z^{-5}(1 - e^{-2z})] \quad (\text{B.25})$$

(These functions are regular at  $z = 0$ , which can be verified by direct expansion of the exponential.)

The calculation of the response is also quite simple. We define the impulse response by

$$R_\phi(k, t, t_w) = \left. \frac{\delta}{\delta(\beta h_{\mathbf{k}}(t_w))} \langle \rho_{\mathbf{k}}(t) \rangle \right|_{h=0} = - \left\langle \phi_{\mathbf{k}}(t) \left. \frac{\delta S}{\delta(\beta h_{\mathbf{k}}(t_w))} \right|_{h=0} \right\rangle$$

where  $h_{\mathbf{k}}(t_w)$  is the Fourier transform of the instantaneous perturbation  $h(\mathbf{r})$  which acts at time  $t_w$ .

Substituting directly for the derivative of  $S$ , the terms that contribute at tree level are of the form

$$R_\phi(k, t, t_w) = (Nl_0^d)^{-1} \langle \phi_{\mathbf{k}}(t) \bar{\phi}_{-\mathbf{k}}(t_w) W[\phi(t_w)] \rangle, \quad (\text{B.26})$$

where  $\bar{\phi}_{-\mathbf{k}}(t_w) W[\phi(t_w)]$  contains the terms in  $\frac{\delta S}{\delta h_{\mathbf{k}}(t_w)}$  that are linear in  $\bar{\phi}$ . Evaluating this correlation function at the saddle point, we have  $R_\phi(k, t, t_w) = G_k(t, t_w) W[\langle \phi(t_w) \rangle]$ . and hence

$$R_\phi(k, t, t_w) = 2\lambda[z_k(t_w) - 2]n(t_w)^3 G_k(t, t_w) \quad (\text{B.27})$$

Evaluating the FDR by taking a derivative of the correlation, we arrive at

$$\begin{aligned} X_\phi(k, t, t_w) &\equiv \frac{R_\phi(k, t, t_w)}{\partial_{t_w} C_\phi(k, t, t_w)} \\ &= \frac{-2 + z_k(t_w)}{\left\{ 1 + g_k + z_k(t_w) \left[ 1 + \frac{d}{dz_k(t_w)} \right] \right\}} F[z_k(t_w), g_k] \end{aligned} \quad (\text{B.28})$$

where we note that the FDR is independent of  $t$ , and depends on  $k$  and  $t_w$  only through the scaling variable  $z_k(t_w)$ .

As discussed in the main text, the relevant limits for the SPM aging regime are  $k\ell \ll 1$ ,  $k^2 \gg \rho(t_w)$ , and  $\ell^{-2} \ll k^2 \ll \rho(t)$ . These correspond to  $[z_k(t) \ll 1, g_k = 0]$ ,  $[z_k(t_w) \gg 1, g_k = 1]$ , and  $[z_k(t) \ll 1, g_k = 0]$  respectively. Calculating the FDR in these limits leads to

$$X_\phi(k, t, t_w) \equiv \frac{R_\phi(k, t, t_w)}{\partial_{t_w} C_\phi(k, t, t_w)} = \begin{cases} -\frac{5}{2} + \mathcal{O}(z_k(t_w)^{-1}) & [k\ell \ll 1] \\ 1 + \mathcal{O}(z_k(t_w)) & [k^2 \gg \rho(t_w)] \\ -3 + \mathcal{O}(z_k(t_w)^{-1}) & [\ell^{-2} \ll k^2 \ll \rho(t)] \end{cases} \quad (\text{B.29})$$

As expected for a reaction-diffusion system with activated dynamics [27], the large  $k$  response has an FDR of unity, while the response at small  $k$  is negative. The intermediate regime with a well-defined negative FDR is a result of the presence of two length scales in the SPM, both of which grow with time.

## References

- [1] For reviews see, e.g., M. D. Ediger, C. A. Angell and S. R. Nagel, *J. Phys. Chem.* **100** 13200 (1996); C. A. Angell, *Science* **267**, 1924 (1995); P. G. Debenedetti and F.H. Stillinger, *Nature* **410**, 259 (2001).
- [2] L. C. E. Struik, *Physical Aging in Amorphous Polymers and Other Materials*, (Elsevier, Houston, 1978).
- [3] *Spin glasses & random fields*, edited by A.P. Young, (World Scientific, New York, 1998).
- [4] J. P. Garrahan, *J. Phys. Condens. Matter* **14**, 1571 (2002).
- [5] A. Buhot and J. P. Garrahan, *Phys. Rev. Lett.* **88**, 225702 (2002).
- [6] R. L. Jack, L. Berthier and J. P. Garrahan, *Phys. Rev. E* **72**, 016103 (2005).
- [7] R. L. Jack and J. P. Garrahan, *J. Chem. Phys.* **123**, 164508 (2005).
- [8] L. F. Cugliandolo and J. Kurchan, *Phys. Rev. Lett.* **71**, 173 (1993); *J. Phys. A* **27**, 5749 (1994).
- [9] J. Kurchan and L. Laloux, *J. Phys. A* **29**, 1929 (1996).
- [10] L. F. Cugliandolo, J. Kurchan, and L. Peliti, *Phys. Rev. E* **55**, 3898 (1997).
- [11] J. Kurchan, *Nature* **433**, 222 (2005).
- [12] S. Franz, M. Mézard, G. Parisi, and L. Peliti, *Phys. Rev. Lett.* **81**, 1758 (1998).
- [13] A. Crisanti and F. Ritort, *J. Phys. A* **36**, R181 (2003).
- [14] D. S. Fisher and D. A. Huse, *Phys. Rev. Lett.* **56**, 1601 (1986).
- [15] See, for example: K. Schmidt-Rohr and H. Spiess, *Phys. Rev. Lett.* **66**, 3020 (1991); M. T. Cicerone and M. D. Ediger, *J. Chem. Phys.* **103**, 5684 (1995); E. V. Russell and N. E. Israeloff, *Nature* **408**, 695 (2000); E. Weeks et al., *Science* **287**, 627 (2000); W. K. Kegel and A. van Blaaderen, *Science* **287**, 290 (2000); P. Mayer et al., *Phys. Rev. Lett.* **93**, 115701 (2004).
- [16] For reviews, see: H. Sillescu, *J. Non-Cryst. Solids* **243**, 81 (1999); M. D. Ediger, *Annu. Rev. Phys. Chem.* **51**, 99 (2000); S. C. Glotzer, *J. Non-Cryst. Solids*, **274**, 342 (2000); R. Richert, *J. Phys. Condens. Matter* **14**, R703 (2002); H. C. Andersen, *Proc. Natl. Acad. Sci. U. S. A.* **102**, 6686 (2005).
- [17] A. Crisanti, F. Ritort, A. Rocco, and M. Sellitto, *J. Chem. Phys.* **113**, 10615 (2000); P. Viot, J. Talbot, and G. Tarjus, *Fractals* **11**, 185 (2003).
- [18] M. Nicodemi, *Phys. Rev. Lett.* **82**, 3734 (1999).
- [19] F. Krzakala, *Phys. Rev. Lett.* **94**, 077204 (2005).
- [20] A. Buhot, *J. Phys. A* **36**, 12367 (2003).
- [21] J. P. Garrahan and M. E. J. Newman, *Phys. Rev. E* **62**, 7670 (2000).
- [22] S. Fielding and P. Sollich, *Phys. Rev. Lett.* **88**, 050603 (2002).
- [23] P. Mayer, L. Berthier, J. P. Garrahan, and P. Sollich, *Phys. Rev. E* **68**, 016116 (2003); *Phys. Rev. E* **70**, 018102 (2004).
- [24] A. Barrat and L. Berthier, *Phys. Rev. Lett.* **87**, 087204 (2001).
- [25] H. E. Castillo, C. Chamon, L. F. Cugliandolo, and M. P. Kennett, *Phys. Rev. Lett.* **88**, 237201 (2002).
- [26] L. Bellon, S. Ciliberto and C. Laroche, *Europhys. Lett.* **53**, 511 (2001).
- [27] P. Mayer, S. Leonard, L. Berthier, J. P. Garrahan and P. Sollich, *Phys. Rev. Lett.* **96**, 030602 (2006).
- [28] A. Lipowski, *J. Phys. A* **30**, 7365 (1997)
- [29] M. E. J. Newman and C. Moore, *Phys. Rev. E* **60**, 5068 (1999).
- [30] F. Ritort and P. Sollich, *Adv. Phys.* **52**, 219 (2003).
- [31] For studies of other glassy spin models with plaquette interactions, which do not map simply to kinetically constrained models, see for example: D. Alvarez, S. Franz and F. Ritort, *Phys. Rev. B* **54**, 9756 (1996); M. R. Swift, H. Bokil, R. D. M. Travasso and A. J. Bray, *Phys. Rev. B* **62**, 11494 (2000); A. Lipowski and D. Johnston, *Phys. Rev. E* **64**, 041605 (2001); P. Dimopoulos, D. Espriu, E. Jane and A. Prats, *Phys. Rev. E* **66**, 056112 (2002).
- [32] For a review, see P. Calabrese and A. Gambassi, *J. Phys. A* **38**, R133 (2005).

- [33] J. Jäckle and S. Eisinger, *Z. Phys. B* **84**, 115 (1991).
- [34] L. Berthier and J.P. Garrahan, *J. Phys. Chem. B* **109**, 3578 (2005).
- [35] D.J. Ashton, L.O. Hedges and J.P. Garrahan, *J. Stat. Mech.* P12010 (2005).
- [36] P. Sollich and M.R. Evans, *Phys. Rev. Lett.* **83**, 3238 (1999); *Phys. Rev. E* **68**, 031504 (2003).
- [37] G. H. Fredrickson and H. C. Andersen, *Phys. Rev. Lett* **53**, 1244 (1984).
- [38] C. Chatelain, *J. Stat. Mech.* P06006 (2004).
- [39] F. Ricci-Tersenghi, *Phys. Rev. E* **68**, 065104 (2003).
- [40] A. Barrat, *Phys. Rev. E* **57**, 3629 (1998).
- [41] L. Berthier, J.-L. Barrat, and J. Kurchan, *Eur. Phys. J. B* **11**, 635 (1999).
- [42] S. Franz, C. Donati, G. Parisi and S. C. Glotzer, *Phil. Mag. B* **79**, 1927 (1999).
- [43] S. Léonard, P. Mayer, L. Berthier, J.P. Garrahan, and P. Sollich, in preparation.
- [44] M. Schulz and S. Trimper, *J. Stat. Phys.* **94**, 173 (1999).
- [45] S. Whitelam, L. Berthier, and J. P. Garrahan, *Phys. Rev. Lett.* **92**, 185705 (2004); *Phys. Rev. E* **71**, 026128 (2005); see also R. L. Jack, P. Mayer and P. Sollich *J. Stat. Mech* (2006) P03006.
- [46] B. P. Lee, *J. Phys. A* **27**, 2633 (1994).
- [47] U. C. Täuber, M. Howard, and B. P. Vollmayr-Lee, *J. Phys. A* **38**, R79 (2005).
- [48] M. Doi, *J. Phys. A* **9**, 1479 (1976); L. Peliti, *J. Phys. (Paris)* **46**, 1469 (1984).